J|A|C|S
ARTICLES
Published on Web 10/29/2004

$[Fe_2(SR)_2(\mu\text{-CO})(CNMe)_6]^{2+}$ and Analogues: A New Class of Diiron Dithiolates as Structural Models for the H_{ox}^{Air} State of the Fe-Only Hydrogenase

Christine A. Boyke,[†] Thomas B. Rauchfuss,*[,†] Scott R. Wilson,[†] Marie-Madeleine Rohmer,[‡] and Marc Bénard*[,‡]

Contribution from the Department of Chemistry, University of Illinois, Urbana, Illinois 61801, and Laboratoire de Chemie Quantique, UMR 7551, CNRS and Université Louis Pasteur, F-67000 Strasbourg, France

Received February 19, 2004; E-mail: rauchfuz@uiuc.edu; benard@quantix.u-strasbg.fr

Abstract: Low-temperature oxidation of $Fe_2(S_2C_nH_{2n})(CNMe)_{6-x}(CO)_x$ ($n = 2, 3$; $x = 2, 3$) affords a family of mixed carbonyl-isocyanides of the type $[Fe_2(S_2C_nH_{2n})(CO)_x(CNMe)_{7-x}]^{2+}$. The degree of substitution is controlled by the RNC/Fe ratio, as well as the degree of initial substitution at iron, with tricarbonyl derivatives favoring more highly carbonylated products. The structures of the monocarbonyl derivatives $[Fe_2(S_2C_nH_{2n})(\mu\text{-CO})(CNMe)_6](PF_6)_2$ ($n = 2,3$) established crystallographically and spectroscopically, are quite similar, with Fe---Fe distances of ca. 2.5 Å, although the μ-CO is unsymmetrical in the propanedithiolate derivative. Isomeric forms of $[Fe_2(S_2C_3H_6)(CO)(CNMe)_6](PF_6)_2$ were characterized where the CO is bridging or terminal, the greatest structural difference being the 0.1 Å elongation of the Fe---Fe distance when MeNC (vs CO) is bridging. In the dicarbonyl species, $[Fe_2(S_2C_2H_4)(\mu\text{-CO})(CO)(CNMe)_5](PF_6)_2$, the terminal CO ligand is situated at one of the basal sites, not trans to the Fe---Fe vector. Oxidation of $Fe_2(S_2C_2H_4)(CNMe)_3(CO)_3$ under 1 atm CO gives the deep pink tricarbonyl $[Fe_2(S_2C_2H_4)(CO)_3(CNMe)_4](PF_6)_2$. DFT calculations show that a bridging CO or MeNC establishes a 3-center, 2-electron bond within the two Fe(II) centers, which would otherwise be nonbonding.

Introduction

The biological processing of hydrogen[1] is exceptionally efficient, with rates for proton reduction in the range of 6000−9000 turnovers/s and dihydrogen oxidation of 10^4 turnovers/s.[2,3] Understanding the mechanism of the hydrogenases begins with replicating the structure of their active sites, which have been determined to good precision by single-crystal X-ray diffraction,[3−6] the main problem being the possible cocrystallization of different oxidation states of the enzyme. The active site of the Fe-only hydrogenases has attracted specific attention of the modeling community[7−9] because it resembles well-known species of the general formula $Fe_2(SR)_2(CO)_{6-x}L_x$, which can be generated and manipulated by well-established synthetic methods.

The H_2-binding centers in the Fe-only hydrogenases[4−6,10,11] adopt a face-shared bi-octahedral structure (Figure 1). The entire complement of ancillary ligands (Figure 1) are unusual in the biological context.[12] Cyanide and CO are rarely observed in Nature, although they are also found in the NiFe hydrogenases.[13] Other unusual features include the dithiolate cofactor, the sulfur atoms of which bridge the iron atoms,[14,15] and an $Fe_4S_4(SR)_4$ cluster that is linked to the active site via a cysteinyl thiolate bridge.[16,17] In toto, the oxidized, active form (H_{ox}, see below) of the binuclear active site can be described as $[Fe_2[(SCH_2)_2X](CN)_2(\mu\text{-CO})(CO)_2(SR_2)(L)]^z$, where SR_2 represents the thiolato-bridged Fe_4S_4 ligand, X is speculated to be NH, and L is the H_x-binding site ($x = 1, 2$) that can also be occupied by CO (H_{ox}^{CO}) and possibly H_2O.[5,18]

The active site is proposed to exist in three oxidation states, H_{red}, H_{ox}, and H_{ox}^{air} (Figure 1).[2,11,19,20] H_{red} and H_{ox} are

[†] University of Illinois.
[‡] CNRS and Université Louis Pasteur.

(1) Cammack, R.; Frey, M.; Robson, R. *Hydrogen as a Fuel; Learning From Nature*; Taylor and Francis: London and New York, 2001.
(2) Adams, M. W. W. *Biochim. Biophys. Acta* **1990**, *1020*, 115−145.
(3) Frey, M. *ChemBioChem.* **2002**, *3*, 153−160.
(4) Nicolet, Y.; Piras, C.; Legrand, P.; Hatchikian, C. E.; Fontecilla-Camps, J. C. *Structure* **1999**, *7*, 13−23.
(5) Peters, J. W.; Lanzilotta, W. N.; Lemon, B. J.; Seefeldt, L. C. *Science* **1998**, *282*, 1853−1858.
(6) Lemon, B. J.; Peters, J. W. *Biochemistry* **1999**, *38*, 12969−12973.
(7) Evans, D. J.; Pickett, C. J. *Chem. Soc. Rev.* **2003**, *32*, 268−275.
(8) Darensbourg, M. Y.; Lyon, E. J.; Zhao, X.; Georgakaki, I. P. *Proc. Natl. Acad. Sci. of U.S.A.* **2003**, *100*, 3683−3688.
(9) Rauchfuss, T. B. *Inorg. Chem.* **2004**, *43*, 14−26.
(10) Lemon, B. J.; Peters, J. W. *J. Am. Chem. Soc.* **2000**, *122*, 3793−3794.
(11) Nicolet, Y.; de Lacey, A. L.; Vernède, X.; Fernandez, V. M.; Hatchikian, E. C.; Fontecilla-Camps, J. C. *J. Am. Chem. Soc.* **2001**, *123*, 1596−1601.
(12) Pierik, A. J.; Roseboom, W.; Happe, R. P.; Bagley, K. A.; Albracht, S. P. J. *J. Biol. Chem.* **1999**, *274*, 3331−3337.
(13) Volbeda, A.; Fontecilla-Camps, J. C. *Dalton Trans.* **2003**, 4030−4038.
(14) Nicolet, Y.; de Lacey, A. L.; Vernede, X.; Fernandez, V. M.; Hatchikian, E. C.; Fontecilla-Camps, J. C. *J. Am. Chem. Soc.* **2001**, *123*, 1596−1601.
(15) Li, H.; Rauchfuss, T. B. *J. Am. Chem. Soc.* **2002**, *124*, 726−727.
(16) Holm, R. H. *Pure Appl. Chem.* **1995**, *67*, 217−224.
(17) Beinert, H.; Holm, R. H.; Munck, E. *Science* **1997**, *277*, 653−659.
(18) Bennett, B.; Lemon, B. J.; Peters, J. W. *Biochemistry* **2000**, *39*, 7455−7460.
(19) Pierik, A. J.; Hulstein, M.; Hagen, W. R.; Albracht, S. P. J. *Eur. J. Biochem.* **1998**, *258*, 572−578.

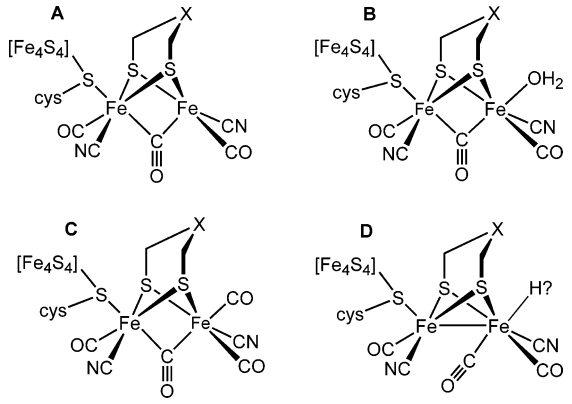

Figure 1. Structures proposed for the four states of the active site of Fe H_2-ase: (A) H_{ox}, (B) H_{ox}^{air}, (C) H_{ox}^{CO}, (D) H_{red}.

catalytically active. The as-isolated, air-denatured state, H_{ox}^{air}, requires reduction to restore activity. Spectroscopic measurements and DFT calculations indicate that H_{red} is a diamagnetic diiron(I) species whereas H_{ox} features an $S = 1/2$ $Fe^p(II)Fe^d(I)$ center,[21,22] where Fe^p and Fe^d refer respectively to the metals that are proximal and distal with respect to the [4Fe−4S] cluster. It is interesting that the substrate binding (distal) metal is proposed to maintain the Fe(I) oxidation state in both H_{red} and H_{ox} states. Consistent with this picture, H_{ox}^{air} is diamagnetic, as expected for an $[Fe(II)]_2$ species bound to strong field ligands. Mössbauer studies are, however, also consistent with $[Fe(II)]_2$ and Fe(II)Fe(III) for H_{red} and H_{ox}, respectively.[23]

Initial synthetic modeling of the binuclear active site was focused on cyano-substituted derivatives of diiron dithiolates, e.g., $[Fe_2(S_2C_3H_6)(CN)_2(CO)_4]^{2-}$ and related azadithiolato analogues $[Fe_2[(SCH_2)_2NR](CN)_2(CO)_4]^{2-}$ (R = H, Me).[24−27] Related compounds with bridging hydrides replicate aspects of the H_2-producing[28] and H−D exchange properties of the hydrogenases.[29,30] The azadithiolate cofactor has also been generated on a diiron carbonyl.[15,31] *The bridging CO ligand has, however, resisted modeling efforts*. The elusiveness of $[Fe_2(SR)_2(\mu\text{-CO})L_6]^{z+}$ species is remarkable given the vast amount of research on the Fe−SR−CO system.[32,33] The absence of the μ-CO functionality may indicate that prior models have failed to generate the binuclear site in the biologically relevant oxidation state. This "oxidation state gap" between synthetic models and the natural system may explain functional deficiencies in synthetic models, i.e., the absence of H_2 complexes, the absence of thermal H_2-D_2O exchange, and the absence of terminal hydrides (vs the isomeric μ-hydrides, which are well-precedented[34]). We suggest that progress in modeling of the structure of the binuclear site will lead to breakthroughs in function.

Pickett et al. showed that the $Fe_2(\mu\text{-CO})$ entity is stabilized at higher oxidation states. Thus, one-electron oxidation of $[Fe_2[\kappa^2\text{-}(SCH_2)_2C(Me)CH_2SMe\}(CN)_2)(CO)_4]^{2-}$ generates a spectroscopically characterized transient $[Fe_2\{\kappa^3\text{-}(SCH_2)_2C(Me)\text{-}CH_2SMe\}(\mu\text{-CO})(CN)_2(CO)_3]^-$, which decomposes above −40 °C (eq 1).[35]

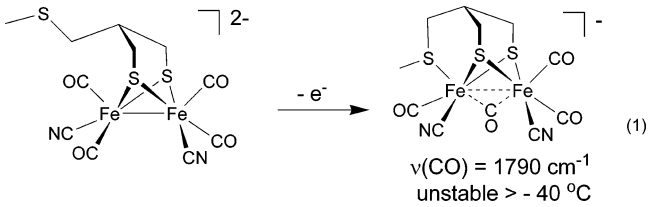

Our approach to hydrogenase modeling involves addressing the H_{ox}^{air} state, which once replicated, would be amenable to conversion to models for the active H_{ox} state. A promising lead is our finding that oxidation of the electron-rich species $Fe_2(S_2C_nH_{2n})(CO)_2(CNMe)_4$ in the presence of CNMe generates $[Fe_2(S_2C_nH_{2n})(\mu\text{-CNMe})(CNMe)_6]^{2+}$.[36] Although mechanistic aspects of these redox reactions require further study, the point of immediate attention is that the structures of the resulting dications resemble the coordination geometry of the CO-inhibited form of H_{ox}, i.e., H_{ox}^{CO} (eq 2).[6]

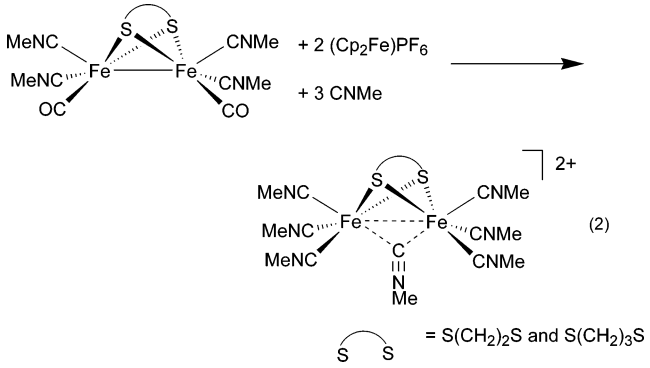

In contrast to H_{ox}^{CO}, however, these dications are diamagnetic d^6-d^6 species, thus these species closely replicate H_{ox}^{air}. Given that CNR is isoelectronic with CO, it follows that one should be able to generate $[Fe_2(S_2C_nH_{2n})(CO)_x(CNMe)_{7-x}]^{2+}$, incorporating the μ-CO ligand that is so characteristic of the oxidized forms of the active site, H_{ox}, H_{ox}^{CO}, and H_{ox}^{air}. As we describe in this paper, stable derivatives of such previously elusive bridging carbonyl complexes can be prepared by selective oxidation of $Fe_2(S_2C_nH_{2n})(CO)_{6-x}(CNMe)_x$, where $x = 2$ and 3. These, the first structural models of H_{ox}^{air}, have

(20) Chen, Z.; Lemon, B. J.; Huang, S.; Swartz, D. J.; Peters, J. W.; Bagley, K. A. *Biochemistry* **2002**, *41*, 2036−2043.
(21) Liu, Z.-P.; Hu, P. *J. Am. Chem. Soc.* **2002**, *124*, 5175−5182.
(22) Cao, Z.; Hall, M. B. *J. Am. Chem. Soc.* **2001**, *123*, 3734−3742.
(23) Huynh, B. H.; Tavares, P.; Pereira, A. S.; Moura, I.; Moura, J. J. G. In *Biochemistry and Physiology of Anaerobic Bacteria*; Lujungdahl, L. G., Adams, M. W., Barton, L. L., Ferry, J. G., Johnson, M. K., Eds.; Springer: New York, 2003.
(24) Schmidt, M.; Contakes, S. M.; Rauchfuss, T. B. *J. Am. Chem. Soc.* **1999**, *121*, 9736−9737.
(25) Lyon, E. J.; Georgakaki, I. P.; Reibenspies, J. H.; Darensbourg, M. Y. *Angew. Chem., Int. Ed. Engl.* **1999**, *38*, 3178−3180.
(26) Le Cloirec, A.; Best, S. P.; Borg, S.; Davies, S. C.; Evans, D. J.; Hughes, D. L.; Pickett, C. J. *Chem. Commun.* **1999**, 2285−2286.
(27) Lawrence, J. D.; Li, H.; Rauchfuss, T. B.; Bénard, M.; Rohmer, M.-M. *Angew Chem., Int. Ed. Engl.* **2001**, *40*, 1768−1771.
(28) Gloaguen, F.; Lawrence, J. D.; Rauchfuss, T. B.; Bénard, M.; Rohmer, M.-M. *Inorg. Chem.* **2002**, *41*, 6573−6582.
(29) Gloaguen, F.; Lawrence, J. D.; Rauchfuss, T. B. *J. Am. Chem. Soc.* **2001**, *123*, 9476−9477.
(30) Zhao, X.; Georgakaki, I. P.; Miller, M. L.; Yarbrough, J. C.; Darensbourg, M. Y. *J. Am. Chem. Soc.* **2001**, *123*, 9710−9711.
(31) Lawrence, J. D.; Li, H.; Rauchfuss, T. B. *Chem. Commun.* **2001**, 1482−1483.
(32) Reihlen, H.; Friedolsheim, A. v.; Ostwald, W. *Justus Liebigs Ann. Chem.* **1928**, *465*, 72−96.
(33) Seyferth, D.; Womack, G. B.; Dewan, J. C. *J. Organomet. Chem.* **1985**, *281*, 111−118.
(34) Arabi, M. S.; Mathieu, R.; Poilblanc, R. *J. Organomet. Chem.* **1979**, *177*, 199−209.
(35) Razavet, M.; Borg, S. J.; George, S. J.; Best, S. P.; Fairhurst, S. A.; Pickett, C. J. *Chem. Commun.* **2002**, 700−701.
(36) Lawrence, J. D.; Rauchfuss, T. B.; Wilson, S. R. *Inorg. Chem.* **2002**, *41*, 6193−6195.

Scheme 1

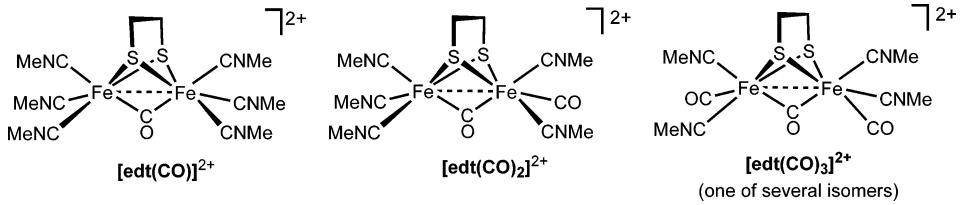

been characterized spectroscopically and crystallographically, and their bonding and stabilities have been analyzed by DFT calculations.

Results and Discussion

Synthesis and Characterization. Preparative work began with a systematic examination of the oxidation of $Fe_2(S_2C_3H_6)(CNMe)_4(CO)_2$ in the presence of MeNC. Previously, we showed that this reaction gives mainly $[Fe_2(S_2C_3H_6)(CNMe)_7]^{2+}$ together with significant amounts of $\{(C_3H_6S_2)[Fe(CNMe)_5]_2\}^{2+}$. We have found that the course of the oxidation is sensitive to the following experimental conditions: light, temperature, the degree of pre-substitution of the diiron dithiolate (i.e., $Fe_2(S_2C_nH_{2n})(CO)_3(CNMe)_3$ vs $Fe_2(S_2C_nH_{2n})(CO)_2(CNMe)_4$), and the amount of free MeNC. Attention to these factors has allowed the preparation of the targeted $Fe_2(\mu\text{-CO})$ derivatives. Results obtained for the ethanedithiolate and propanedithiolate derivatives differ subtly but significantly and are presented in separate sections, beginning with the ethanedithiolate species.

Ethanedithiolates $[Fe_2(S_2C_2H_4)(CO)_x(CNMe)_{7-x}]^{2+}$. Products obtained are listed in Scheme 1.

Low-temperature oxidation of $Fe_2(S_2C_2H_4)(CNMe)_4(CO)_2$ in the presence of CNMe with $FcPF_6$ in MeCN solution gave 30% yield of analytically pure $[Fe_2(S_2C_2H_4)(\mu\text{-CO})(CNMe)_6](PF_6)_2$, **[edt(CO)]**$(PF_6)_2$. The ^{1}H NMR spectrum of this salt confirmed its C_{2v} symmetric structure (Figure 2). Its IR spectrum exhibits

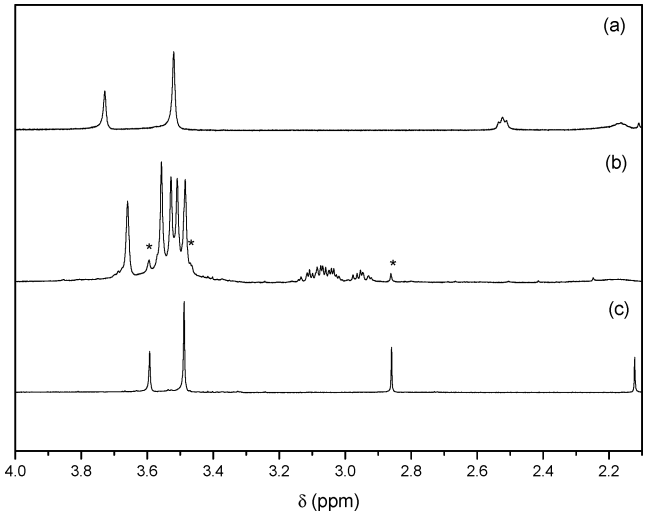

Figure 2. 500 MHz ^{1}H NMR spectra (CD_3CN soln, ambient temperature) of $[Fe_2(S_2C_3H_6)(\mu\text{-CO})(CNMe)_6](PF_6)_2$ (a), $[Fe_2(S_2C_2H_4)(\mu\text{-CO})(CO)(CNMe)_5](PF_6)_2$ (b), and $[Fe_2(S_2C_2H_4)(\mu\text{-CO})(CNMe)_6](PF_6)_2$ (c). Peaks marked with * are assigned to $[Fe_2(S_2C_2H_4)(\mu\text{-CO})(CNMe)_6](PF_6)_2$.

ν_{CO} at 1914 cm^{-1} (Figure 3). In the absence of light, MeCN solutions of **[edt(CO)]**$^{2+}$ are stable for days at room temperature.

Oxidation of *tri*carbonyl $Fe_2(S_2C_2H_4)(CNMe)_3(CO)_3$ in the presence of *fewer* equiv of CNMe gave ca. 30% yield of the *dicarbonyl* $[Fe_2(S_2C_2H_4)(\mu\text{-CO})(CO)(CNMe)_5](PF_6)_2$, **[edt(CO)$_2$]**$(PF_6)_2$ (Scheme 1). Due to the photosensitivity of the dicarbonyl, it was necessary to conduct the workup in the absence of light. ^{1}H NMR spectroscopy indicates that the five MeNC ligands in **[edt(CO)$_2$]**$^{2+}$ are nonequivalent (Figure 2), which uniquely fixes the stereochemistry provided that one CO is bridging. The ^{1}H NMR spectrum for the $S_2C_2H_4$ portion of the spectrum consists of a complex multiplet, also consistent with a low symmetry structure. The IR spectrum of **[edt(CO)$_2$]**$(PF_6)_2$ consists of ν_{CO} bands at 2051 and 1941 cm^{-1} (Figure 3).

Even in the dark, MeCN solutions of **[edt(CO)$_2$]**$^{2+}$ decarbonylate over the course of days to produce mainly **[edt(CO)]**$^{2+}$ as demonstrated by IR analysis. Apparently such a conversion requires the sacrifice of some of the diiron complexes with liberation of MeNC; indeed, this conversion is more efficient upon the addition of one equiv MeNC. UV-photolysis of a solution of **[edt(CO)$_2$]**$^{2+}$ and MeNC produced $[Fe_2(S_2C_2H_4)(CNMe)_7]^{2+}$ within minutes.

The synthesis of $[Fe_2(S_2C_2H_4)(\mu\text{-CO})(CN^tBu)_6](PF_6)_2$ was performed under conditions analogous to those for **[edt(CO)]**$(PF_6)_2$. The product mixture was complex and optimization was not pursued. Crystallographic characterization of $[Fe_2(S_2C_2H_4)(\mu\text{-CO})(CN^tBu)_6](PF_6)_2$ confirmed the resemblance of this species to the corresponding **[edt(CO)]**$(PF_6)_2$ (see below).

In contrast to the preceding reaction, oxidation of the *tri*carbonyl $Fe_2(S_2C_2H_4)(CNMe)_3(CO)_3$ in the absence of free

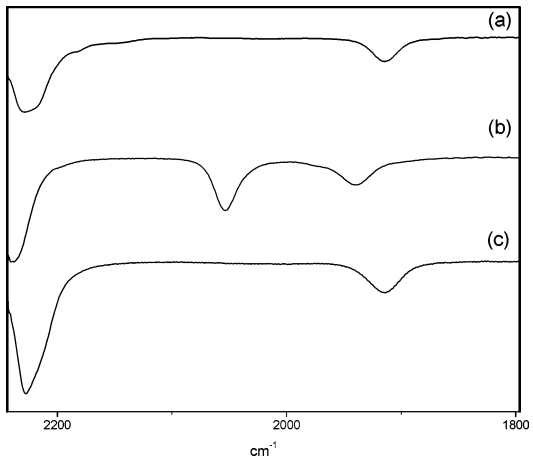

Figure 3. IR spectra (MeCN soln) $[Fe_2(S_2C_3H_6)(\mu\text{-CO})(CNMe)_6](PF_6)_2$ (a), $[Fe_2(S_2C_2H_4)(\mu\text{-CO})(CO)(CNMe)_5](PF_6)_2$ (b), and $[Fe_2(S_2C_2H_4)(\mu\text{-CO})(CNMe)_6](PF_6)_2$ (c). Bands >2100 cm^{-1} are assigned to ν_{CN}.

CNMe but under 1 atm CO gave the deep pink tricarbonyl $[Fe_2(S_2C_2H_4)(CO)_3(CNMe)_4](PF_6)_2$, **[edt(CO)$_3$]**$(PF_6)_2$ together with **[edt(CO)$_2$]**$(PF_6)_2$. The IR spectrum of the tricarbonyl features ν_{CO} bands at 2089, 2072, and 1968 cm^{-1}. ESI−MS also revealed a peak at 597 *m*/*z* corresponding to $\{[Fe_2(S_2C_2H_4)(CO)_3(CNMe)_4](PF_6)\}^+$ as well as at 610 *m*/*z* for $\{[Fe_2(S_2C_2H_4)(CO)_2$-

Scheme 2

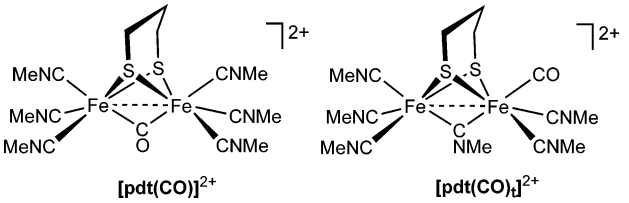

$(CNMe)_5](PF_6)\}^+$. These oxidations were conducted in $MeNO_2$ solution because $[\mathbf{edt(CO)_3}]^{2+}$ decomposes in MeCN solution to give $\mathbf{edt(CO)_2}^{2+}$. We were unable to separate $[\mathbf{edt}(CO)_2](PF_6)_2$ from $[\mathbf{edt(CO)_3}](PF_6)_2$, due to their similar properties and the sensitivity of the tricarbonyl to most solvents. The ratio $[\mathbf{edt(CO)_3}]^{2+}/[\mathbf{edt(CO)_2}]^{2+}$ increased when the oxidation was conducted under 4 atm of CO. The tetrasubstituted derivative $Fe_2(S_2C_2H_4)(CO)_2(CNMe)_4$ was found to be a poorer precursor to $[\mathbf{edt(CO)_3}](PF_6)_2$ than $Fe_2(S_2C_2H_4)(CO)_3(CNMe)_3$, showing that the CO capture by the initially oxidized species is less efficient than is capture of CNMe.

Propanedithiolates: $[Fe_2(S_2C_3H_6)(CO)_x(CNMe)_{7-x}]^{2+}$. Low-temperature oxidation of $Fe_2(S_2C_3H_6)(CNMe)_3(CO)_3$ in the presence of MeNC with substoichiometric $FcPF_6$ gave a 34% isolated yield of analytically pure $[Fe_2(S_2C_3H_6)(\mu\text{-CO})(CNMe)_6](PF_6)_2$, ($[\mathbf{pdt(CO)}](PF_6)_2$,see Scheme 2). Additional equiv of Fc^+ resulted in higher conversions, but the products also contained $[Fe_2(S_2C_3H_6)(CO)_x(CNMe)_{7-x}](PF_6)_2$, where $x = 2$, 3 ($\nu_{CO} = 2087, 2071, 2047, 1984, 1947\ cm^{-1}$). Thus the initial equivs of Fc^+ attack the more easily oxidized, MeNC-rich derivatives.

Characterization of $[\mathbf{pdt(CO)}](PF_6)_2$ rests on ESI−MS and NMR measurements, which confirmed the formula unit and its idealized C_{2v} symmetry, respectively (Figure 2). The ν_{CO} band at 1914 cm^{-1} (1914 cm^{-1} in the solid state) is very similar to that for $[\mathbf{edt(CO)}](PF_6)_2$, which is noteworthy because the solid-state structures of the two compounds differ with respect to the symmetry of the μ-CO. In the absence of light, MeCN solutions of $[\mathbf{pdt(CO)}](PF_6)_2$ are stable for days at room temperature.

Oxidation of $Fe_2(S_2C_3H_6)(CO)_{6-x}(CNMe)_x$ ($x = 2$, 3) in the presence of only 1.5−2 equiv of MeNC (vs 2.6 equiv) afforded mixtures, the IR spectrum of which indicated the presence of ν_{COt} but not $\nu_{\mu-CO}$. The ESI−MS of this mixture revealed peaks at 637 and 624 m/z corresponding to $\{[Fe_2(S_2C_3H_6)(CO)(CNMe)_6](PF_6)\}^+$ and $\{[Fe_2(S_2C_3H_6)(CO)_2(CNMe)_5](PF_6)\}^+$, respectively. From one preparation we were able to obtain single crystals of the unsymmetrical isomer $[Fe_2(S_2C_3H_6)(\mu\text{-CNMe})(CO)(CNMe)_5](PF_6)_2$ ($[\mathbf{pdt(CO)_t}](PF_6)_2$), which contains a single terminal CO. This salt was characterized by IR and NMR spectroscopies as well as by mass spectrometry and X-ray crystallography (see below). MeCN solutions of $[\mathbf{pdt(CO)_t}]^{2+}$ showed no tendency to isomerize to $[\mathbf{pdt(CO)}]^{2+}$ prior to decomposition ($t_{1/2} \approx 48$ h) as determined by IR spectroscopy.

Crystallographic Studies. Crystallographic analyses of $[Fe_2(S_2C_nH_{2n})(CO)(CNMe)_6](PF_6)_2$ ($n = 2$, 3) revealed the expected diiron species with idealized C_{2v} symmetry (Figure 4, Table 1). Two $Fe(CNMe)_3$ centers are bridged by CO and two thiolato sulfur atoms. The most conspicuous difference between the two structures is the degree of asymmetry of the Fe-μ-CO distances, Δ(Fe−C). For $[\mathbf{edt(CO)}](PF_6)_2$, Δ(Fe−C) is only 0.006 Å, whereas Δ(Fe−C) is 0.095 Å for $[\mathbf{pdt(CO)}](PF_6)_2$. For both CO-bridged species, the Fe−Fe distances of 2.490 and 2.503

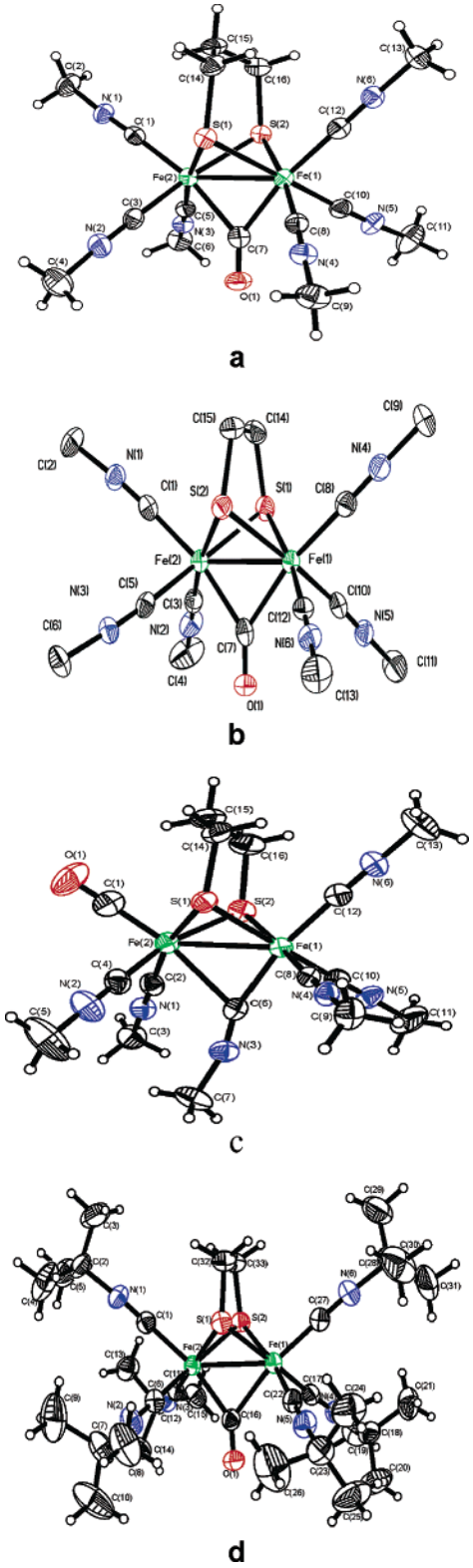

Figure 4. Crystallographic structures of the dications in $[Fe_2(S_2C_2H_4)(\mu\text{-CO})(CNMe)_6](PF_6)_2$ (a), $[Fe_2(S_2C_3H_6)(\mu\text{-CO})(CNMe)_6](PF_6)_2$ (b), $[Fe_2(S_2C_3H_6)(\mu\text{-CNMe})(CO)(CNMe)_5](PF_6)_2$ (c), and $[Fe_2(S_2C_2H_4)(\mu\text{-CO})(CN^tBu)_6](PF_6)_2$ (d). Thermal ellipsoids represent the 50% probability level.

Å, respectively, are shorter by ∼0.1 Å than in $[Fe_2(S_2C_nH_{2n})(\mu\text{-CNMe})(CNMe)_6](PF_6)_2$ (Table 1).[36] Previous structural studies on pairs of analogous μ-CO and μ-CNR complexes have revealed little effect. For example, in $Cp_2Fe_2(CO)_2(\mu\text{-CO})_2$ and $Cp_2Fe_2(CO)_2(\mu\text{-CNMe})_2$, the Fe−Fe distances are indistinguish-

Table 1. Selected Bond Lengths (Å) for $[Fe_2(S_2C_nH_{2n})(Co)_x(CNMe)_{7-x}](PF_6)_2$ and Related Species

	Fe–Fe	Fe1–S1	Fe1–S2	Fe2–S1	Fe2–S2	Fe1–μC	Fe2–μC	reference
$[Fe_2(S_2C_2H_4)(CO)(CNMe)_6](PF_6)_2$	2.49	2.257	2.248	2.258	2.255	1.99	1.984	this work
$[Fe_2(S_2C_3H_6)(CO)(CNMe)_6](PF_6)_2$	2.503	2.259	2.260	2.268	2.273	1.947	2.042	this work
$[Fe_2(S_2C_2H_4)(CNMe)_7](PF_6)_2$	2.600	2.250	2.277	2.250	2.277	2.078	2.078	27
$[Fe_2(S_2C_3H_6)(CNMe)_7](PF_6)_2$	2.634	2.235	2.270	2.290	2.301	2.3	1.952	27
$[Fe_2(S_2C_3H_6)(\mu\text{-}CNMe)(CO)(CNMe)_5](PF_6)_2$	2.629	2.296	2.297	2.231	2.244	1.916	2.381	this work
$[Fe_2(S_2C_2H_4)(CO)(^tBuNC)_6](PF_6)_2$	2.494	2.348	2.248	2.259	2.265	2.061	1.933	this work
active site of *C. pasteurianum*	2.61	2.34	2.31	2.31	2.33	2.09	2.04	5

Table 2. Relative Energies (ΔE, kcal·mol^{-1}) and Selected Geometrical Parameters (Distances in Å, Angles in °) Calculated for $[Fe_2(S_2C_3H_6)(\mu\text{-L})(R)_6]^{2+}$ (L, R = CNH, CNMe, CO) at Various Positions of the Bridging Ligand[a]

	L = CNH R = CNH	L = CNMe R = CNH	L = CNMe R = CNH	L = CNMe R = CNH	L = CNMe R = CNH	L = CNMe R = CNMe	L = R = CNMe (obs)	L = none R = CNH
Fe1−C	1.961	1.969	2.037[b]	2.105[c]	2.174	1.960	1.952	
Fe2−C	2.146	2.242	2.186	2.105[c]	1.969[b]	2.226	2.300	
Fe1−Fe2	2.571	2.636	2.631	2.629	2.620	2.625	2.634	2.923
Fe1−S	2.318	2.332	2.323	2.309	2.295	2.325	2.296[d]	2.344
Fe2−S	2.293	2.290	2.301	2.311	2.325	2.290	2.253[d]	2.285
∠CNR	140.4	162.8	177.0	180.0	179.9	164.0	168.3	
$\theta_2 - \theta_1$	8.4	11.2	8.4	4.7	0.8	9.9	9.35	10.2
ΔE		+0.6	0.0	+0.3	+1.3			

	L = CO R = CNH	L = CO R = CNH	L = CO R = CNH	L = CO R = CNH	L = CO R = CNMe (obs)	L = CNH R = CO,[e] CNH (calcd)	L = CNH R = CO,[f] CNH (calcd)	L = CNMe R = CO,[f] CNMe (obs)
Fe1−C	1.880[b]	1.955	2.014[c]	2.097	1.947	2.023	1.925	1.915
Fe2−C	2.170	2.089	2.014[c]	1.880[b]	2.042	2.082	2.289	2.378
Fe1−Fe2	2.566	2.556	2.558	2.545	2.503	2.579	2.627	2.629
Fe1−S	2.324	2.316	2.305	2.288	2.271	2.312	2.329	2.298
Fe2−S	2.286	2.297	2.308	2.323	2.260	2.297	2.282	2.237
∠CNR						143.2	151.5	
$\theta_2 - \theta_1$	11.3	7.6	4.6	0.3	6.7	8.0	10.3	14.5
ΔE	+0.4	0.0	+0.35	+1.7		−0.4	−1.5	

[a] Geometrical parameters observed for **[pdt(CNMe)]**$^{2+}$ and for **[pdt(CO)]**$^{2+}$ (this work) are specified.[36] [b] Constrained value. [c] Fe1−C and Fe2−C constrained to be equal. [d] Average. [e] Terminal CO on Fe1. This isomer has not been observed experimentally. [f] Terminal CO on Fe2.

able.[37,38] The Fe−Fe bond lengths of $Fe_2(CO)_9$ and $Fe_2(CNEt)_9$ are 2.523 and 2.461 Å, respectively.[39,40] Our results suggest that Δ(Fe−C) for μ-CO vs μ-CNR is more pronounced at higher oxidation states.

Crystallographic analysis of $[Fe_2(S_2C_2H_4)(\mu\text{-CO})(CN^tBu)_6](PF_6)_2$ confirmed its close similarity to **[edt(CO)]**$(PF_6)_2$, although Δ(Fe−C) has increased from negligible to 0.128 Å. The C−N−C angles for the ^{t}BuNC ligands range from 168 to 175° vs 175−180° for MeNC. The Fe−Fe distance at 2.49 Å resembles that for the three other μ-CO species.

Our previous crystallographic analysis of $[Fe_2(S_2C_3H_6)(\mu\text{-CNMe})(CNMe)_6](PF_6)_2$ revealed an asymmetrically bridging isocyanide with a $\Delta(Fe-C_\mu) = 0.35$ Å, vs only 0.095 Å for the aforementioned **[pdt(CO)]**$(PF_6)_2$. In the unsymmetrical isomer of **[pdt(CO)$_t$]**$(PF_6)_2$ (Figure 4c), $\Delta Fe-C\mu$ is larger still at 0.463 Å.

The Fe−Fe bond length of the new μ-CO species, ca. 2.5 Å is similar to the bond length observed in more reduced species such as $[Fe_2(S_2C_2H_4)(CN)_2(CO)_4]^{2-}$ (2.5116 Å).[24] More electronically relevant are dimanganese analogues: $Mn_2(S_2C_2H_4)(CO)_7$ and $Mn_2(SMe)_2(\mu\text{-CO})(PMe_3)_2(CO)_4$ have M−M bond lengths of 2.65 and 2.58 Å, respectively.[41,42] The corresponding Mn−μ-C distances are 1.956 and 2.23 Å and 1.985 and 2.027 Å, respectively. Crystallographically characterized $[Fe(II)]_2$ species include the protonated $[HFe_2(S_2C_3H_6)_2(PMe_3)_2(CO)_4]^+$ and $[HFe_2(S_2C_3H_6)_2(CN)(PMe_3)(CO)_4]$ where $d_{Fe-Fe} = 2.58$ Å and $d_{Fe-COt} = 1.78$ Å.[30,43,44]

DFT Calculations on $[Fe_2(S_2C_nH_{2n})(\mu\text{-L})(CNR)_6]^{2+}$ (L = CNH, CNMe, CO; R = H, Me). A number of models of Fe-only hydrogenase involving dithiolate-bridged complexes of Fe(I)−Fe(I), Fe(I)−Fe(II) and Fe(II)−Fe(II), with various terminal ligands and, in most cases, a bridging or semi-bridging carbon monoxide have been recently the subject of theoretical investigations.[22,45−53] Cationic complexes of the type $[Fe_2(S_2C_nH_{2n})(\mu\text{-L})(CNR)_6]^{2+}$ ($n = 2, 3$) are composed of two FeL_5 fragments sharing the bridging dithiolate ligand and completing their coordination sphere with a bridging CO or CNMe ligand characterized either in symmetrically bridging or in semi-bridging position. The FeL_5 fragments form an approximate square pyramid with the base defined by a C_2S_2 donor set. In

(37) Mitschler, A.; Rees, B.; Lehmann, M. S. *J. Am. Chem. Soc.* **1978**, *100*, 3390−3397.
(38) Cotton, F. A.; Frenz, B. A. *Inorg. Chem.* **1974**, *13*, 253−256.
(39) Cotton, F. A.; Troup, J. M. *J. Chem. Soc., Dalton Trans.* **1974**, 800−802.
(40) Bassett, J. M.; Barker, G. K.; Green, M.; Howard, J. A. K.; Stone, F. G. A.; Wolsey, W. C. *J. Chem. Soc., Dalton Trans.* **1981**, 219−227.
(41) Adams, R. D.; Kwon, O. S.; Smith, M. D. *Isr. J. Chem.* **2001**, *41*, 197−206.
(42) Lyons, L. J.; Tegen, M. H.; Haller, K. J.; Evans, D. H.; Treichel, P. M. *Organometallics* **1988**, *7*, 357−365.
(43) Savariault, J. M.; Bonnet, J. J.; Mathieu, R.; Galy, J. *Comptes Rendus C: Sci. Chim.* **1977**, *284*, 663−665.
(44) Gloaguen, F.; Lawrence, J. D.; Rauchfuss, T. B.; Bénard, M.; Rohmer, M.-M. *Inorg. Chem.* **2002**, *41*, 6573−6582.
(45) Lyon, E. J.; Georgakaki, I. P.; Reibenspies, J. H.; Darensbourg, M. Y. *J. Am. Chem. Soc.* **2001**, *123*, 3268−3278.
(46) Dance, I. *Chem. Commun.* **1999**, 1655−1656.
(47) Liu, Z.-P.; Hu, P. *J. Am. Chem. Soc.* **2002**, *124*, 5175−5182.
(48) Georgakaki, I. P.; Thomson, L. M.; Lyon, E. J.; Hall, M. B.; Darensbourg, M. Y. *Coord. Chem. Rev.* **2003**, *238−239*, 255−266.
(49) Liu, Z.-P.; Hu, P. *J. Chem. Phys.* **2002**, *117*, 8177−8180.
(50) Fan, H.-J.; Hall, M. B. *J. Am. Chem. Soc.* **2001**, *123*, 3828−3829.
(51) Bruschi, M.; Fantucci, P.; De Gioia, L. *Inorg. Chem.* **2002**, *41*, 1421−1429.
(52) Bruschi, M.; Fantucci, P.; De Gioia, L. *Inorg. Chem.* **2004**, *43*, 4733.
(53) Bruschi, M.; Fantucci, P.; De Gioia, L. *Inorg. Chem.* **2003**, *42*, 4773−4781.

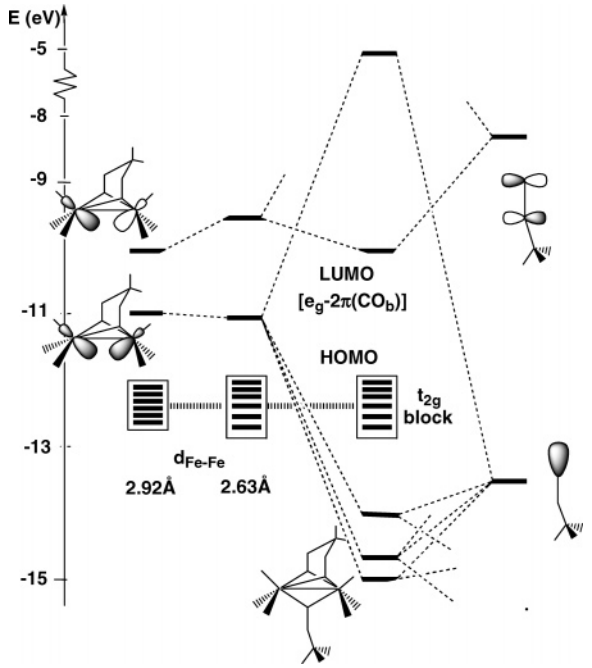

Figure 5. $[Fe_2(S_2C_3H_6)(\mu\text{-CNMe})(CNH)_6]^{2+}$: Fragment interaction diagram, from EHMO calculations. Left hand-side: frontier orbitals of the $[Fe_2(S_2C_3H_6)(CNH)_6]^{2+}$ fragment, (i) at the equilibrium Fe−Fe distance calculated with DFT for the isolated fragment (2.92 Å), and (ii) at the equilibrium Fe−Fe distance calculated in the complex (2.63 Å). Fe1−C and Fe2−C distances have been assumed identical (2.105 Å).

this geometry, the e_g set of metal orbitals splits such that the d_{z^2}-like orbital is stabilized relative to its $d_{x^2-y^2}$ counterpart.[54] At this point, it is important to note that the relative environment of the two Fe atoms in $[Fe_2(S_2C_nH_{2n})(CNR)_6]^{2+}$ is influenced by the alkyl bridge connecting the sulfur atoms. The ethanedithiolate is symmetric with respect to a plane perpendicular to the Fe−Fe axis and the environments of both metals are strictly equivalent. The propanedithiolate bridge is nonplanar and a weak steric interaction develops between the apical CH_2 and one CNR ligand, resulting in some tilting of the underlying $Fe(CNR)_3$ tripod and the associated d_{z^2}-like orbital (Scheme 3). The

Scheme 3

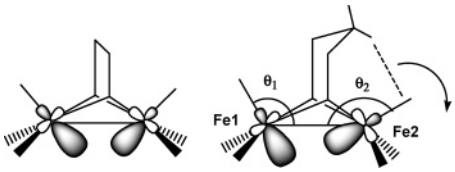

Δ(Θ)	Compound
6.7	$[\mathbf{pdt(CO)}]^{2+}$
9.3	$[\mathbf{edt(CNMe)}]^{2+}$
14.5	$[\mathbf{pdt(CO)_t}]^{2+}$

amplitude of this tilt appears surprisingly variable in a series of compounds exhibiting similar steric strain. A difference of 6.7° between θ_1 and θ_2 is observed for $[\mathbf{pdt(CO)}]^{2+}$, but $\Delta\theta$ increases to 9.3° in $[Fe_2(S_2C_3H_6)(\mu\text{-CNMe})(CNMe)_6]^{2+}$ and reaches 14.5° in $[\mathbf{pdt(CO)_t}]^{2+}$ (Table 2). In a similar way, the steric influence of the bent μ-*o*-xylyldithiolate ligand on the dynamic behavior of an underlying $Fe_2(CO)_6$ unit has been recently documented by Lyon et al.,[45] whereas calculations by Liu and Hu indicated that the asymmetry of μ-CO is influenced by *attractive* interactions between the amine in the azadithiolate cofactor and adjacent apical ligands.[47]

In the dicationic, Fe^{II} complexes, each iron is d^6 and the 12 combined metal electrons are accommodated in the six in-phase

(54) Albright, T. A.; Burdett, J. K.; Whangbo, M. H. *Orbital Interactions in Chemistry*; Wiley: New York, 1985.

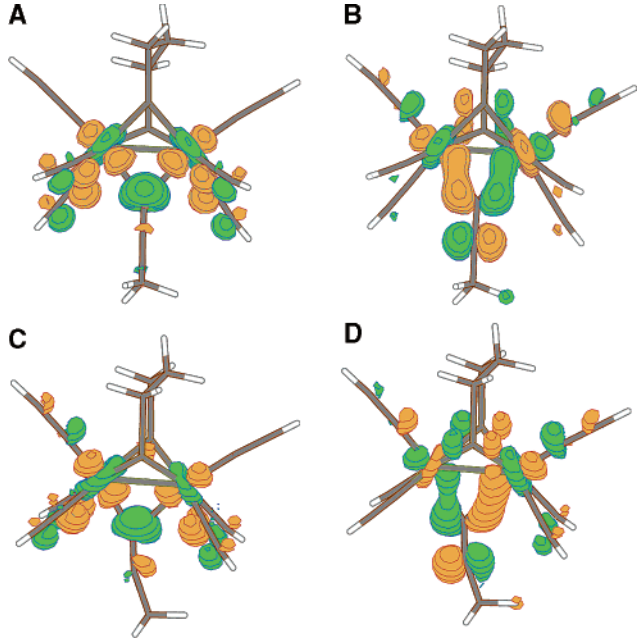

Figure 6. MOLDEN plots of some unoccupied Kohn−Sham molecular orbitals illustrating the interactions between μ-CNMe and the di-iron moiety in $[Fe_2(S_2C_3H_6)(\mu\text{-CNMe})(CNH)_6]^{2+}$: (A) LUMO+3, symmetric; (B) LUMO, symmetric; (C) LUMO+3, semi-bridging; (D) LUMO, semi-bridging. See also text and Figure 5.

and out-of-phase combinations of the t_{2g} sets. Consequently no net metal−metal bond would exist for the hypothetical species $[Fe_2(S_2C_nH_{2n})(CNR)_6]^{2+}$ wherein all CNR ligands are terminal. The Fe−Fe bonding orbital, represented in Scheme 3, is the LUMO. Geometry optimization carried out on the model system $[Fe_2(S_2C_3H_6)(CNH)_6]^{2+}$ confirms the absence of an Fe−Fe bond: the equilibrium Fe−Fe distance is calculated to be 2.92 Å. *Introducing an additional ligand with σ/π donor character in the bridging position between the metals activates a strong, stabilizing interaction between the ligand donor orbitals and the Fe−Fe bonding LUMO of the complex* (Scheme 4). The

Scheme 4

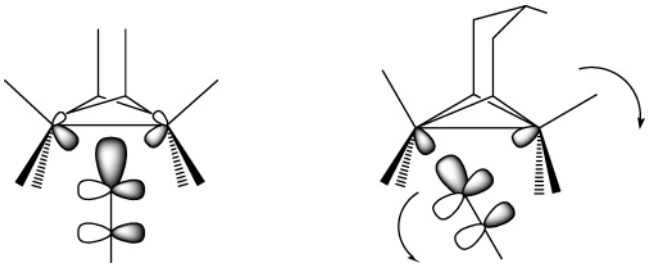

importance of this interaction is illustrated by the orbital diagram of Figure 5, obtained from extended Hückel (EHMO) calculations. The stabilized orbital, with predominant ligand lone pair character, lies rather deep in energy and is split into several components due to weak four-electron interactions (Figure 5). The strength of the interaction is also indicated by the high energy of its metal−ligand antibonding counterpart. In contrast with the bonding orbital, this orbital is largely unaffected by side interactions, in both the EHMO and DFT analyses. The composition of the appropriate Kohn−Sham unoccupied orbital (the LUMO+3, Figure 6A,C), reflects the antibonding nature of the Fe−C−Fe interaction and the gradual change of its

composition as the CNMe ligand bends toward Fe1. Note, however, that the bending hardly modifies the orbital energy and the overall strength of the interaction. As a consequence of this interaction, the metal e_g orbital with Fe−Fe σ-antibonding character becomes the LUMO and is somewhat stabilized due to an interaction with the π^* orbital of the central ligand (Figure 5). This relatively low-lying orbital, unoccupied in Fe(II)−Fe(II) systems, but partly or fully occupied in reduced complexes, has been previously referred to by Liu and Hu as the e_g-$2\pi(CO_b)$ MO.[47]

Strong back-donation interactions are also evidenced between the metal t_{2g} combinations and the ligand π^* orbitals. The donation and back-donation interactions appear balanced for semi-bridging CNMe, whereas for semi-bridging CNH back-donation is more important.[55] As a consequence of this difference in Fe-μ-CNR back-donation is manifested in the shorter bond length between the semi-bridged CNH and the weakly bound Fe vs the CNMe case (Table 2). The bond strength between the $[Fe_2(S_2C_3H_6)(CNH)_6]^{2+}$ fragment and the bridging ligand was calculated to be 49.2 kcal·mol^{-1} for CO, 58.0 kcal·mol^{-1} for CNH, and 61.5 kcal·mol^{-1} for CNMe.[55]

Addition of the ligand across the Fe---Fe vector dramatically contracts the Fe−Fe distance to values compatible with a metal−metal single bond. This change is readily explained by the formation of a two-electron/three-center bond involving the two metal atoms and the ligand. This two-electron/three-center bond involves *either* the ligand lone pair if the ligand is symmetrically bridging or this lone pair orbital *and* one π orbital if this ligand is semi-bridging (Scheme 4).

The similar strength of the two bonding modes provides the ligand with a structural flexibility that has been already noticed in previous experimental and theoretical studies.[11,22,36,45−48] Geometry optimizations were carried out on $[Fe_2(S_2C_3H_6)(\mu\text{-CNMe})(CNH)_6]^{2+}$ and $[Fe_2(S_2C_3H_6)(\mu\text{-CO})(CNH)_6]^{2+}$ constraining the bridging ligand to occupy various positions from symmetrically bridging to semi-bridging. Varying the position of the inserted ligand from symmetric ($d_{Fe1-C} = d_{Fe2-C}$) to semi-bridging, tilted toward Fe1, involves practically no change in the molecular energy (Table 2).

This facile tilting of the bridging ligand should account for the observed sensitivity of the μ-CNMe or μ-CO ligand position to the slight dissymmetry introduced when replacing $S_2C_2H_4$ by $S_2C_3H_6$. As illustrated in Schemes 3 and 4, this minor dissymmetry induces a tilting of the Fe2-$(CNR)_3$ tripod, which in turn displaces the central ligand into a semi-bridging position. The energies of the interacting orbitals and the total molecular energy are just slightly affected by relatively large back and forth displacements of the central ligand R (Table 2). With R = CNH or CO, the calculated minimum is obtained with a significant bending of R toward Fe1 (Table 2). A marked correlation is obtained between the semi-bridging character of the inserted ligand, measured either by $\Delta(\text{Fe-}\mu\text{C}) = d_{Fe1-\mu C} - d_{Fe2-\mu C}$ or by the angular difference $\Delta(\angle\text{FeCX})$, and the angular difference $\Delta\theta = \theta_1 - \theta_2$ in the bending of the $Fe(CNR)_3$ tripods (Table 2). $\Delta\theta$ is computed to be small, but nonzero (4.7°) with μ-L = μ-CNMe case, 4.6° with μ-L = μ-CO) when the inserted ligand is constrained to symmetrically bridge the diiron complex. Tilting μ-L toward Fe1 facilitates the bending of the Fe_2L_3 tripod and increases $\Delta\theta$ up to 10° and even beyond, but an equivalent tilt in the opposite direction (i.e. toward Fe2) just yields $\Delta\theta$ close to zero (Table 2). The comparison between the structures observed for $[Fe_2(S_2C_3H_6)(\mu\text{-CNMe})(CNMe)_6]^{2+}$ and $[\mathbf{pdt}\text{-}(CO)]^{2+}$ provides an experimental confirmation of the correlation between $\Delta(\text{Fe}-\mu\text{C})$ and $\Delta\theta$. In the former complex, an important tilting of μ-CNMe ($\Delta(\text{Fe}-\mu\text{C}) = 0.35$ Å) is associated with a value of 9.35° for $\Delta\theta$. It is interesting to note that a similar value of $\Delta\theta \approx 10°$ was computed for the hypothetical unbridged complex $[Fe_2(S_2C_3H_6)(CNMe)_6]^{2+}$. It therefore seems that for this complex the position of the inserted ligand is strongly influenced by the steric interactions in the coordination sphere of Fe2. However, the tilting of μ-CO in $[\mathbf{pdt(CO)}]^{2+}$ remains moderate ($\Delta(\text{Fe}-\mu\text{C}) = 0.095$ Å), and $\Delta\theta$ is reduced to 6.7° (Table 2). Conversely, in the $[\mathbf{pdt(CO)_t}]^{2+}$, which has a terminal CO ligand, μ-CNMe tilts further to a quasi-terminal coordination mode on Fe1 (Fe1−μC = 1.915 Å, $\Delta(\text{Fe}-\mu\text{C}) =$ 0.46 Å), and $\Delta\theta$ has soared to 14.5°. A tentative explanation invokes an increased trans-effect associated with terminal CO repelling the bridging isocyanide toward Fe1. This is consistent with observed and computed structural data indicating that d_{Fe-C} is significantly shorter for terminal CO than for terminal CNH or CNMe.

Another structural correlation can be observed and confirmed from the calculations between $\Delta(\text{Fe}-\mu\text{C})$ and $\Delta(\text{FeS})$ ($= d_{Fe1-S} - d_{Fe2-S}$). Constraining the bridging ligand, either μ-CO or μ-CNR to be symmetric ($\Delta(\text{Fe-}\mu\text{C}) = 0$) leads to a near identity of the four Fe−S distances, i.e., $\Delta(\text{FeS}) \approx 0$ (Table 2). Displacement of μ-L toward Fe1 is associated with an elongation of the Fe1−S distances. Conversely, the Fe−S bond lengths contract at Fe2, resulting in a distance gap $\Delta(\text{FeS})$ of 0.043 Å in $[Fe_2(S_2C_3H_6)(\mu\text{-CNMe})(CNMe)_6]^{2+}$, well reproduced by the calculations (Table 2). $\Delta(\text{FeS})$ is relatively large in $pdt(CO)^{2+}$ (observed 0.061 Å with L = Me; computed 0.047 Å with L = H), a compound characterized by an extreme tilting of μ-CNR. Calculations also show that constraining μ-L to bend *toward Fe2* reverses the sign of $\Delta(\text{FeS})$ (Table 2). However, the Fe−S distance gap should not be assigned only to the semi-bridging coordination, since calculations show that this gap is maximal in the hypothetical unbridged complex $[Fe_2(S_2C_3H_6)(CNH)_6]^{2+}$ with an amplitude of 0.059 Å (Table 2). Therefore, the Fe−S distances are also sensitive to the distortions induced in the coordination spheres of Fe1 and Fe2 by the bending and by the deformation of the $Fe(CNR)_3$ tripods.

In $[\mathbf{pdt(CO)}]^{2+}$, the tilting of the μ-CNMe toward the *opposite* iron atom would yield a less efficient overlap between the ligand donor orbitals and the LUMO of the dithiolate complex. To optimize this overlap, $\Delta\theta$ would need to be further reduced to ~0°, thus increasing the steric repulsion between the apical CH_2 group and the underlying ligand. It should, however, be kept in mind that these ligand displacements occur on a very flat potential energy surface, where small energy differences can induce large structural modifications. The relative energies associated with a tilt of μ-L in the direction opposite to that of maximal stability are indeed higher, but do not exceed +1.3 kcal·mol^{-1} for μ-CNMe (d_{Fe2-C} fixed at 1.97 Å) and +1.7 kcal·mol^{-1} for μ-CO (d_{Fe2-C} fixed at 1.97 Å) (Table 2).

(55) CNH calculated in a tilted conformation (d_{Fe1-C} constrained to 1.96 Å, $d_{Fe2-C} = 2.146$ Å) is strongly bent (<CNH = 140.4°) and d_{CN} elongated by 0.023 Å with respect to free CNH. Donation and back-donation appear more balanced with CNMe ($d_{Fe1-C} = 1.969$ Å, $d_{Fe2-C} = 2.242$ Å, <CNC = 162.8°, ΔCN = 0.007 Å).

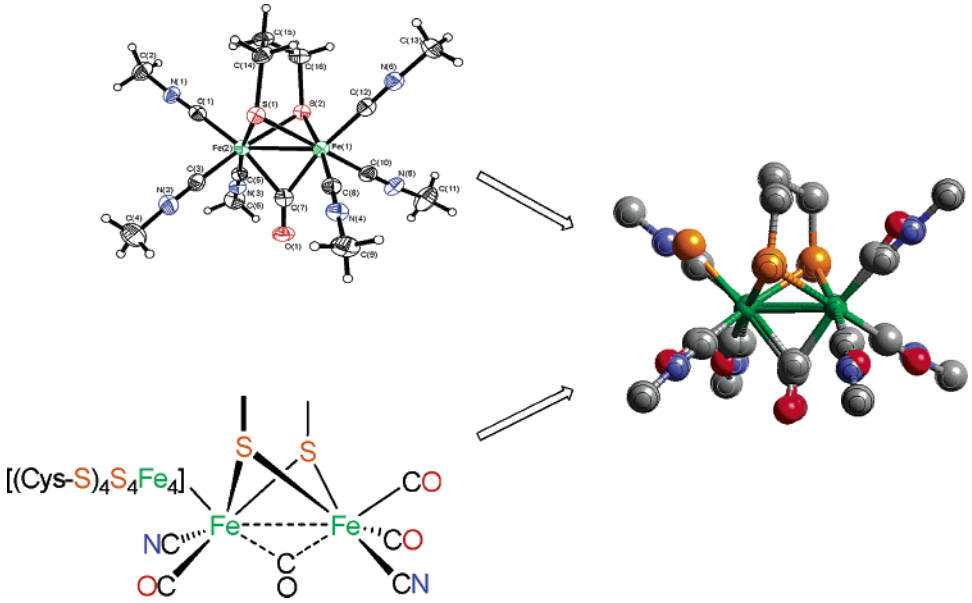

Figure 7. Overlay of the crystallographic models of the dication in $[Fe_2(S_2C_3H_6)(CO)(CNMe)_6](PF_6)_2$ with the binuclear active site in the CO-inhibited form of *C. pasteurianum* (CpI) Fe-only hydrogenase, where all the diatomic ligands were labeled as CO (red terminal atoms) in the H-cluster. The central XH_n atom of the dithiolate backbone was not included nor was the Fe_4S_4 cluster. The positions for $[Fe_2(S_2C_3H_6)(CO)(CNMe)_6]^{2+}$ are indicated by striped atoms. Legend: C, gray, Fe, green, N, blue, O, red, S, orange.

For the isomer of $[Fe_2(S_2C_3H_6)(\mu\text{-CO})(CNMe)_6]^{2+}$ in which the bridging carbonyl and one CNR ligand coordinated to Fe2 have been interchanged, calculations on the $[Fe_2(S_2C_3H_6)(\mu\text{-CNH})(CNH)_5(CO)]^{2+}$ model predict this isomer to be only marginally more stable than the μ-CO form (-1.5 kcal·mol^{-1}). The observed bending of μ-CNMe toward Fe1 is more pronounced than in $[Fe_2(S_2C_3H_6)(\mu\text{-CNMe})(CNMe)_6]^{2+}$. This large bending was reproduced by the calculations and assigned to the trans influence of the terminal CO. This interpretation is supported by the optimized structure for the hypothetical isomer of $[Fe_2(S_2C_3H_6)(\mu\text{-CNH})(CNH)_5(CO)]^{2+}$ in which terminal CO is attached to Fe1. The stability of this isomer is comparable to that of the μ-CO form (-0.4 kcal·mol^{-1}), but the μ-CNH ligand is now displaced *away* from Fe1 when compared to $[Fe_2(S_2C_3H_6)(\mu\text{-CNH})(CNH)_6]^{2+}$ (Table 2).

Discussion

The aim of this work was to lay the preparative foundation for systematic studies on diferrous dithiolates containing μ-CO ligands. Otherwise, very substantial bodies of work exist for $(Fe^{III})_2S_2L_4$ species[17] and $(Fe^{I})_2(SR)_2(CO)_{6-x}L_x$ ($x = 0, 1, 2$). Using isocyanides as illustrative donor ligands, we have developed syntheses of mixed ligand diferrous dithiolate complexes of the general type $[Fe_2(SR)_2(CO)_{7-x}L_x]^{2+}$. Ongoing studies indicate that the range of donor ligands can be expanded well beyond CNR.[56] Furthermore, the new dications should be amenable to ligand substitution reactions. Mononuclear metal carbonyl cations exhibit high reactivity,[57] although few studies have examined the corresponding reactivity of dimetal carbonyl cations.

The new synthetic methodology affords compounds whose structures faithfully reproduce the geometry of the binuclear core of the H_{ox}^{CO} state of Fe H_2-ases.[6] An overlay of the enzyme active site of the H_{ox}^{CO} form of the enzyme from *C. pasteurianum* and the **[pdt(CO)]**$^{2+}$ is shown in Figure 7 (see also Table 1). Crystallographic characterization of H_{ox}^{air} has not been reported,[3] but indications are that it structurally resembles H_{ox}, although it is diamagnetic.

Further conclusions from this work are as follows:

(1) The dithiolate cofactor significantly influences the geometry of the other ligands. Crystallographic results in combination with DFT calculations highlight the significant influence of the propanedithiolate on the structure of the underlying Fe_2L_7 framework, even if these structural changes reflect an energetically shallow surface. Propanedithiolate is isostructural with the biological cofactor, whereas ethanedithiolate provides a convenient reference ligand due to its small steric profile and the quasi-planarity of its backbone.

(2) Theory also sheds light on the Fe---Fe interaction, which in $Fe^{II}_2(SR)_2L_6$, of idealized C_{2v} symmetry, should be nonbonding ($\sim$2.9 Å). The bridging ligand enables a three-center, two-electron interaction consistent with a $\sim$2.6 Å Fe---Fe distance as observed in the enzymes in all oxidation states, including the CO-inhibited form.

(3) A noteworthy spectroscopic feature for these new complexes is $\nu_{\mu-CO}$. For the series $[Fe_2(S_2C_3H_6)(\mu\text{-CO})(CNMe)_{6-x}(CO)_x]$, $\nu_{\mu-CO} = 1914$, 1940, and 1968 cm^{-1} for $x = 0$, 1, 2, respectively. Typically values of $\nu_{\mu-CO}$ fall in the range 1750$-$1850 cm^{-1}. Among the rare species exhibiting high $\nu_{\mu-CO}$ frequencies are the binuclear manganese complexes such as $Mn_2(S_2C_2H_4)(CO)_7$ ($\nu_{\mu-CO} = 1902$ cm^{-1}).[41,58] Although it is widely appreciated that high values for ν_{CO} are characteristic of higher oxidation state derivatives, the present results suggest that the ν_{CO} for μ-CO ligands is even more sensitive to oxidation state than are terminal CO ligands.[59]

(4) A discrepancy exists between $\nu_{\mu-CO}$ seen in our models (>1900 cm^{-1}) and the $\nu_{\mu-CO}$ for the H_{ox}^{air} state of the enzyme

(56) Boyke, C. D.; Rauchfuss, T. B.; van der Vlugt, J. I.; Wilson, S. R. *in preparation.*
(57) Willner, H.; Aubke, F. *Organometallics* **2003**, *22*, 3612−3633.
(58) Adams, R. D.; Kwon, O. S.; Smith, M. D. *Inorg. Chem.* **2001**, *40*, 5322−5323.
(59) Braterman, P. S. *Metal Carbonyl Spectra*; Academic Press Inc.: London, 1975.

($\nu_{\mu-CO}$ = 1847 cm^{-1}),[11,19] which is 45 cm^{-1} above that for the CO-inhibited, oxidized enzyme, H_{ox}^{CO} ($\nu_{\mu-CO}$ = 1802 cm^{-1}).[60] The discrepancy between $\nu_{\mu-CO}$ values seen in this work and those in H_{ox}^{air} contrasts with the excellent structural congruence of the fist coordination spheres. Further work on more electron-rich diferrous models are being pursued to close the spectroscopic gap.

Experimental Section

General Procedures. CNMe[61,62] and $FcPF_6$[61,62] were prepared by literature methods. $Fe_2(SR)_2(CO)_6$ was prepared with minor variations from literature methods[63] as described previously.[28] Instrumentation has been previously described.[44] MeCN and Et_2O were purified by degassing with nitrogen purge and were filtered through two 1-m columns of active alumina. Toluene was distilled from molten sodium. Nitromethane was dried over $CaCl_2$.

Crystallography. Crystals were mounted to a thin glass fiber using oil (Paratone-N, Exxon). Data were filtered to remove statistical outliers. The integration software (SAINT) was used to test for crystal decay as a bilinear function of X-ray exposure time and sine(θ). Data were collected at 198 K on a Siemens CCD diffractometer. Crystal and refinement details are given in supplementary information. The structures were solved using SHELXTL by direct methods; correct atomic positions were deduced from an *E* map or by an unweighted difference Fourier synthesis. H atom *U*'s were assigned as 1.2 times the U_{eq}'s of adjacent C atoms. Non-H atoms were refined with anisotropic thermal coefficients. Successful convergence of the full-matrix least-squares refinement of F_2 was indicated by the maximum shift/error for the last cycle.

Computational Details. Calculations were carried out using the formalism of the density functional theory (DFT) within the generalized gradient approximation (GGA), as implemented in the ADF program.[64−67] The exchange-correlation functional used in the calculations is currently referred to as BP86. In this formalism, nonlocal corrections due to Becke for the exchange energy[68,69] and to Perdew for the correlation[70,71] energy have been added to the standard local spin density functional based upon the electron gas exchange and the Vosko−Wilk−Nusair parametrization for correlation.[72] For first row atoms (C, N, O) the 1s shell was frozen and described by a single Slater function. The frozen core of heavier atoms, neon-like for S and argon-like for Fe, was also modeled by a minimal Slater basis. For all nonmetal atoms, the Slater basis set used for the valence shell is of triple-ζ quality and supplemented with one polarization function. The 3s and 3p shells of Fe are described by a double-ζ Slater basis; the 3d and 4s, by a triple-ζ basis, and the 4p shell is described by a single orbital.[73,74]

$[Fe_2(S_2C_2H_4)(\mu\text{-}CO)(CNMe)_6](PF_6)_2$. An orange solution of 0.10 g (0.27 mmol) of $Fe_2(S_2C_2H_4)(CO)_6$ and 0.12 mL (2.2 mmol) of CNMe in 20 mL of MeCN was heated at 70 ± 10 °C for 20 h. The IR spectrum of the resulting deep red solution revealed bands at 1969, 1915, and 1896 cm^{-1} corresponding to $Fe_2(S_2C_2H_4)(CO)_2(CNMe)_4$ and smaller amounts of $Fe_2(S_2C_2H_4)(CO)_3(CNMe)_3$. The reaction solution was cooled to −40 °C and treated with a solution of 0.165 g (0.504 mmol) of Cp_2FePF_6 in 5 mL of MeCN with exclusion to light followed by stirring for 2 min. further. The volume of the resulting green solution was reduced in vacuo to ca. 5 mL at room temperature. Addition of 50 mL of Et_2O was added to precipitate a green solid leaving a red-orange solution of Cp_2Fe and unreacted $Fe_2(S_2C_2H_4)(CO)_{6-x}(CNMe)_x$. The green solid was purified by dissolution in 5 mL of MeCN followed by the addition of 50 mL of Et_2O. Yield: 0.061 g (30%). Anal. Calcd for $C_{15}H_{22}N_6F_{12}Fe_2O_1P_2S_2$: C, 23.45; H, 2.89; N, 10.94. Found: C, 23.00; H, 2.66; N, 10.56. ^1H NMR (CD_3CN): d 3.59 (s, 6H, CNCH_3), 3.49 (s, 12H, CNCH_3), 2.86 (s, 4H, SCH_2). IR (MeCN, cm^{-1}): ν_{CN} = 2228; ν_{CO} = 1914. (KBr, cm^{-1}) ν_{CN} = 2228; ν_{CO} = 1902. ESI−MS (*m*/*z*): 623 ({$[Fe_2(S_2C_2H_4)(CO)(CNMe)_6](PF_6)$}$^+$).

$[Fe_2(S_2C_2H_4)(CO)_2(CNMe)_5](PF_6)_2$. In an aluminum wrapped flask, an orange solution of 0.10 g (0.27 mmol) of $Fe_2(S_2C_2H_4)(CO)_6$ and 0.08 mL (1.5 mmol) of CNMe in 20 mL of MeCN was heated at 70 ± 10 °C for 20 h. The reaction solution was cooled to −40 °C and then treated with a solution of 0.16 g (0.48 mmol) of Cp_2FePF_6 in 5 mL of MeCN with exclusion to light followed by stirring for an additional 2 min. The volume of resulting red-brown solution was reduced to ca. 5 mL in vacuo at room temperature. Addition of 50 mL of Et_2O precipitated a purple solid leaving a brown-orange solution containing $Fe_2(S_2C_2H_4)(CO)_3(CNMe)_3$ and Cp_2Fe. The purple solid was recrystallized by extraction into 5 mL of MeCN followed by the addition of 50 mL of Et_2O. Yield: 0.092 g (42%). Anal. Calcd for $C_{14}H_{19}N_5F_{12}Fe_2O_2P_2S_2$: C, 22.27; H, 2.54; N, 9.27. Found: C, 22.20; H, 2.31; N, 9.15. ^1H NMR (CD_3CN): d 3.66 (s, 3H, CNCH_3), 3.56 (s, 3H, CNCH_3), 3.53 (s, 3H, CNCH_3), 3.51 (s, 3H, CNCH_3), 3.48 (s, 3H, CNCH_3), 3.07 (m, SCH_2), 2.95 (m, SCH_2). IR (MeCN, cm^{-1}): ν_{CN} = 2239; ν_{CO} = 2052, 1939. ESI−MS (*m*/*z*): 610 ({$[Fe_2(S_2C_2H_4)(CO)_2(CNMe)_5](PF_6)$}$^+$).

UV-photolysis (Spectroline MB-100 UV Lamp, 120 V; λ_{max} = 365 nm) of a solution of $[Fe_2(S_2C_2H_4)(CO)_2(CNMe)_5](PF_6)_2$ (0.05 g, 0.06 mmol) and 1 equiv MeNC (0.003 mL, 0.06 mmol) in 10 mL MeCN (quartz flask) produced mainly $[Fe_2(S_2C_2H_4)(CNMe)_7](PF_6)_2$ within 10 min., as monitored by IR spectroscopy.

$[Fe_2(S_2C_2H_4)(CO)(CN^tBu)_6](PF_6)_2$. An orange solution of 0.10 g (0.27 mmol) of $Fe_2(S_2C_2H_4)(CO)_6$ and 0.17 mL (1.5 mmol) of ^{t}BuNC in 20 mL of MeCN was heated to 70 ± 10 °C for 20 h. The resulting red solution was cooled to −40 °C and treated with a solution of 0.16 g (0.48 mmol) of Cp_2FePF_6 in 5 mL of MeCN with exclusion to light; the reaction was stirred for an additional 2 min. The resulting brown/black solution was reduced to ca. 5 mL in vacuo and then diluted with 50 mL of Et_2O to precipitate a brown greasy solid. The solid was extracted into 5 mL of MeCN, and this solution was layered with 50 mL of Et_2O to afford X-ray quality crystals. IR (MeCN, cm^{-1}): ν_{CN} = 2195; ν_{CO} = 2055, 1933, 1908. ESI−MS (*m*/*z*): 875, ({$[Fe_2(S_2C_2H_4)(CO)_2(CN^tBu)_6](PF_6)$}$^+$); 820, ({$[Fe_2(S_2C_2H_4)(CO)_2(CN^tBu)_5](PF_6)$}$^+$).

$[Fe_2(S_2C_2H_4)(CO)_3(CNMe)_4](PF_6)_2$. In an aluminum-wrapped flask, a solution of 0.10 g (0.27 mmol) of $Fe_2(S_2C_2H_4)(CO)_6$ and 0.12 mL (2.2 mmol) of CNMe in 20 mL of MeCN was heated to 70 ± 10 °C for 20 h. The IR spectrum of the resulting deep red solution revealed bands at 1969, 1915 cm^{-1} corresponding to $Fe_2(S_2C_2H_4)(CO)_3(CNMe)_3$.[75] The solvent together with excess CNMe was removed in vacuo. The resulting solid was extracted into 20 mL of $MeNO_2$, which was then continuously saturated with CO and cooled to −35 °C. The stirred reaction mixture was treated with a solution of 0.165 g (0.504 mmol) of Cp_2FePF_6 in 5 mL of $MeNO_2$ with exclusion to light followed

(60) De Lacey, A. L.; Stadler, C.; Cavazza, C.; Hatchikian, E. C.; Fernandez, V. M. *J. Am. Chem. Soc.* **2000**, *122*, 11232−11233.
(61) Schuster, R. E.; Scott, J. E., Jr.; Casanova, J., Jr. *Org. Synth.* **1966**, *46*, 75−77.
(62) Connelly, N. G.; Geiger, W. E. *Chem. Rev.* **1996**, *96*, 877−922.
(63) Winter, A.; Zsolnai, L.; Huttner, G. *Z. Naturforsch.* **1982**, *37b*, 1430−1436.
(64) *ADF 2.3 User's Guide*; Chemistry Department, Vrije Universiteit: Amsterdam, The Netherlands, 1997.
(65) Baerends, E. J.; Ellis, D. E.; Ros, P. *Chem. Phys.* **1973**, *2*, 41−51.
(66) Te Velde, G.; Baerends, E. J. *J. Comput. Phys.* **1992**, *99*, 84−98.
(67) Fonseca-Guerra, C.; Visser, O.; Snijders, J. G.; Baerends, E. J. In *Methods and Techniques in Computational Chemistry: METECC-95*; Clementi, E., Corongiu, G., Eds.; STEF: Cagliari, Italy, 1995; pp 305−395.
(68) Becke, A. D. *Phys. Rev. A: Gen. Phys.* **1988**, *38*, 3098−3100.
(69) Becke, A. D. *J. Chem. Phys.* **1986**, *84*, 4524−4529.
(70) Perdew, J. P. *Phys. Rev.* **1986**, *B33*, 8822−8824.
(71) Perdew, J. P. *Phys. Rev.* **1986**, *B34*, 7406.
(72) Vosko, S. H.; Wilk, L.; Nusair, M. *Can. J. Phys.* **1980**, *58*, 1200−1211.
(73) Snijders, J. G.; Vernooijs, P.; Baerends, E. J. *At. Data Nucl. Data Tables* **1981**, *26*, 483−509.
(74) Vernooijs, P.; Snijders, J. G.; Baerends, E. J. *Slater type basis functions for the whole periodic table*; Vrije Universiteit: Amsterdam, The Netherlands, 1981.
(75) Lawrence, J. D., *Structural and Functional Models of the Iron-only Hydrogenase Enzymes*, Ph.D. Dissertation, University of Illinois at Urbana-Champaign, Urbana, 2002.

by stirring for 2 min. At room temperature, the resulting green solution was concentrated in vacuo to ca. 5 mL. Dilution of this concentrate with 50 mL of Et_2O precipitated a fuchsia-colored oil leaving a yellowish solution containing Cp_2Fe. The oil was purified by dissolution into 5 mL of $MeNO_2$ followed by the addition of 50 mL of Et_2O to yield a purple powder containing both $[Fe_2(S_2C_2H_4)(CO)_3(CNMe)_4]^{2+}$ (~70%) and $[Fe_2(S_2C_2H_4)(CO)_2(CNMe)_5]^{2+}$ (~30%). IR for $[Fe_2(S_2C_2H_4)(CO)_3(CNMe)_4]^{2+}$ ($MeNO_2$, cm^{-1}): $\nu_{CN} = 2244$; $\nu_{CO} = 2089$, 2072, 1969. IR for $[Fe_2(S_2C_2H_4)(CO)_2(CNMe)_5]^{2+}$ ($MeNO_2$, cm^{-1}): $\nu_{CN} = 2244$; $\nu_{CO} = 2052$, 1941. ESI-MS (*m*/*z*): 597 ({$[Fe_2(S_2C_2H_4)(CO)_3(CNMe)_4](PF_6)$}$^+$), 610 ({$[Fe_2(S_2C_2H_4)(CO)_2(CNMe)_5](PF_6)$}$^+$). Repeating the above experiment but under 38 psig CO gave in the same two products with a greater relative proportion of $[Fe_2(S_2C_2H_4)(CO)_3(CNMe)_4]^{2+}$.

$[Fe_2(S_2C_3H_6)(\mu\text{-}CO)(CNMe)_6](PF_6)_2$. A solution of 0.10 g (0.26 mmol) of $Fe_2(S_2C_3H_6)(CO)_6$ and 0.08 mL (1.5 mmol) of CNMe in 20 mL of MeCN was heated at 70 ± 10 °C for 20 h. The IR spectrum of the resulting deep red solution revealed bands at 1969 and 1915 cm^{-1} corresponding to $Fe_2(S_2C_3H_6)(CO)_3(CNMe)_3$.[75] This reaction solution was cooled to −40 °C and treated with a solution of 0.15 g (0.47 mmol) of Cp_2FePF_6 in 5 mL of MeCN with exclusion to light. After 2 min. at −40 °C, the volume of the resulting green solution was reduced in vacuo to ca. 5 mL at room temperature. Addition of 50 mL of Et_2O precipitated a green solid, leaving a red-orange solution of Cp_2Fe and unreacted $Fe_2(S_2C_3H_6)(CO)_{6-x}(CNMe)_x$. The green solid was purified by extraction into 5 mL of MeCN followed by the addition of 50 mL of Et_2O. The precipitate was dissolved in 5 mL of MeCN, and this solution was layered with 20 mL of Et_2O to afford X-ray quality crystals. Yield: 0.07 g (34%). Anal. Calcd for $C_{16}H_{24}N_6F_{12}Fe_2O_1P_2S_2$: C, 24.57; H, 3.09; N, 10.74. Found: C, 24.52; H, 3.07; N, 10.42. ^{1}H NMR (500 MHz, CD_3CN): d 3.70 (s, 6H, CNC*H*$_3$), 3.49 (s, 12H, CNC*H*$_3$), 2.49 (t, 4H, SC*H*$_2$CH$_2$C*H*$_2$S), 2.07 (p, 2H, SCH$_2$C*H*$_2$CH$_2$S). IR (MeCN, cm^{-1}): $\nu_{CN} = 2227$, $\nu_{CO} = 1914$. ESI−MS (*m*/*z*): 636 ({$[Fe_2(S_2C_3H_6)(CO)(CNMe)_6](PF_6)$}$^+$). UV ($MeNO_2$) λ_{max}, nm (ϵ): 300 (5600), 419 (1240), 629 (560).

$[Fe_2(S_2C_3H_6)(\mu\text{-}CNMe)(CO)(CNMe)_5](PF_6)_2$. A solution of 0.10 g (0.26 mmol) of $Fe_2(S_2C_3H_6)(CO)_6$ and 0.06 mL (1.1 mmol) of CNMe in 20 mL MeCN was heated to 70 ±10 °C for 20 h. The IR spectrum of the resulting deep red solution revealed bands at 1969, 1915 cm^{-1} corresponding to $[Fe_2(S_2C_3H_6)(CO)_3(CNMe)_3$.[75] This solution was cooled to −40 °C and treated with a solution of 0.15 g (0.47 mmol) of Cp_2FePF_6 in 5 mL of MeCN with exclusion to light. The solution was allowed to stir for 2 min. at −40 °C before the volume of the resulting green solution was reduced in vacuo to ca. 5 mL at room temperature. Addition of 50 mL of Et_2O precipitated a green solid containing a mixture of products leaving a red-orange solution of Cp_2Fe and unreacted $Fe_2(S_2C_3H_6)(CO)_3(CNMe)_3$. X-ray quality crystals were obtained by layering a MeCN solution of the salt with Et_2O. IR (MeCN, cm^{-1}): $\nu_{CN} = 2215$, $\nu_{CO} = 2002$. ESI−MS (*m*/*z*): 636 ({$[Fe_2(S_2C_3H_6)(CO)(CNMe)_6](PF_6)$}$^+$), 650 ($Fe_2(S_2C_3H_6)(CNMe)_7](PF_6)$}$^+$).

In a separate experiment, a solution of 0.10 g (0.26 mmol) of $Fe_2(S_2C_3H_6)(CO)_6$ in 20 mL MeCN and containing 0.06 mL (1.1 mmol) of CNMe was heated to 70 ± 10 °C for 6 h. The IR spectrum of the resulting deep red solution revealed ν_{CO} bands at 1937, 1971, 2001 cm^{-1} corresponding to $Fe_2(S_2C_3H_6)(CO)_4(CNMe)_2$.[75] This solution was cooled to −40 °C and treated with a solution of 0.15 g (0.47 mmol) of Cp_2FePF_6 in 5 mL of MeCN with exclusion to light. After 2 min. at −40 °C, the volume of the resulting green solution was reduced in vacuo to ca. 5 mL at room temperature. Addition of 50 mL of Et_2O precipitated a green solid containing a mixture of products leaving a red-orange solution of Cp_2Fe and unreacted $Fe_2(S_2C_3H_6)(CO)_3(CNMe)_3$. IR (MeCN, cm^{-1}): $\nu_{CN} = 2227$; $\nu_{CO} = 2060$, 2050, 2021, 2002, 1971-(s). ESI−MS (*m*/*z*): 636 ({$[Fe_2(S_2C_3H_6)(CO)(CNMe)_6](PF_6)$}$^+$), 623 ($Fe_2(S_2C_3H_6)(CO)_2(CNMe)_5](PF_6)$}$^+$).

UV-photolysis of a solution of $[Fe_2(S_2C_3H_6)(\mu\text{-}CO)(CNMe)_6]^{2+}$ (0.05 g, 0.064 mmol) in MeCN under CO resulted in formation of $[Fe_2(S_2C_3H_6)(CNMe)_7]^{2+}$ as analyzed by IR photolysis and some decomposition within a hours. The terminal carbonyl product $[Fe_2(S_2C_3H_6)(\mu\text{-}CNMe)(CO)(CNMe)_5]^{2+}$ was not observed under these conditions.

MeCN solutions of $[Fe_2(S_2C_3H_6)(\mu\text{-}CO)(CNMe)_6]^{2+}$ decompose completely over the course of one week without evidence for conversion to the unsymmetrical isomer $[Fe_2(S_2C_3H_6)(\mu\text{-}CNMe)(CO)(CNMe)_5]^{2+}$.

Acknowledgment. This research was supported by NIH. We thank J. D. Lawrence for advice and assistance at the early stages of this project. DFT calculations were carried out at the IDRIS computer center (Orsay, France).

Supporting Information Available: Optimized geometry tables. Crystallographic information file (cif) for **[pdt(CO)]**-$(PF_6)_2$, **[edt(CO)]**$(PF_6)_2$, **[edt(*t*BuNC)]**$(PF_6)_2$, **[pdt(CO)$_t$]**$(PF_6)_2$. This material is available free of charge via the Internet at http://pubs.acs.org.

JA049050K